Acta Cryst E CRYSTALLOGRAPHIC COMMUNICATIONS

ISSN 2056-9890

Crystal structure, Hirshfeld surface analysis, and DFT and molecular docking studies of 6-cyanonaphthalen-2-yl 4-(benzyloxy)benzoate

Mahadevaiah Harish Kumar,[a] Shivakumar Santhosh Kumar,[b] Hirehalli Chikkegowda Devarajegowda,[a] Hosapalya Thimmaiah Srinivasa[c] and Bandrehalli Siddagangaiah Palakshamurthy[b]*

[a]Department of Physics, Yuvaraja's College, University of Mysore, Mysore, 570005, Karnataka, India, [b]Department of PG Studies and Research in Physics, Albert Einstein Block, UCS, Tumkur University, Tumkur, Karnataka-572103, India, and [c]Raman Research Institute, C. V. Raman, Avenue, Sadashivanagar, Bangalore, Karnataka, India. *Correspondence e-mail: palaksha.bspm@gmail.com

Received 17 September 2024
Accepted 11 October 2024

Edited by M. Weil, Vienna University of Technology, Austria

Keywords: crystal structure; Hirshfeld surface; DFT; 4-(benzyloxy)benzoate; cyanonapthalene and molecular docking; intermolecular interactions.

CCDC reference: 2391127

Supporting information: this article has supporting information at journals.iucr.org/e

In the title compound, $C_{25}H_{17}NO_3$, the torsion angle associated with the phenyl benzoate group is −173.7 (2)° and that for the benzyloxy group is −174.8 (2)° establishing an *anti*-type conformation. The dihedral angles between the ten-membered cyanonaphthalene ring and the aromatic ring of the phenyl benzoate and the benzyloxy fragments are 40.70 (10) and 87.51 (11)°, respectively, whereas the dihedral angle between the aromatic phenyl benzoate and the benzyloxy fragments is 72.30 (13)°. In the crystal, the molecules are linked by weak C—H···O interactions forming $S(4)$ chains propagating parallel to [010]. The packing is consolidated by three C—H···π interactions and two π–π stacking interactions between the aromatic rings of naphthalene and phenyl benzoate with centroid-to-centroid distances of 3.9698 (15) and 3.8568 (15) Å, respectively. Intermolecular interactions were quantified using Hirshfeld surface analysis. The molecular structure was further optimized by density functional theory (DFT) at the B3LYP/6–311+ G(d,p) level, revealing that the energy gap between HOMO and LUMO is 3.17 eV. Molecular docking studies were carried out for the title compound as a ligand and SARS-Covid-2(PDB ID:7QF0) protein as a receptor giving a binding affinity of −9.5 kcal mol^{-1}.

1. Chemical context

Naphthalene derivatives play a vital role in drug design because they have shown to exhibit anti-microbial (El *et al.*, 2018), anti-cancer (Valente *et al.*, 2014), anti-viral (Perrone *et al.*, 2015), anticonvulsant (Özdemir *et al.*, 2019), anti-tubercular (Das *et al.*, 2007), anti-inflammatory (Boyle *et al.*, 1982) and anti-bacterial activities (Ashraf *et al.*, 2019). These properties are attributed to the naphthalene moiety because it is able to disrupt cell membranes, interfere with cell wall synthesis and inhibit enzyme activity. In this context, cyanonaphthalene derivatives have been explored for their possible anti-cancer properties (Hekal *et al.*, 2024). These compounds can cause programmed cell death in cancer cells, which can help slow down tumour growth. They have also been shown to have antifungal activity (Prakash *et al.*, 2015) and to operate as potential inhibitors for the treatment of congestive heart failure and cardiac fibrosis (Voets *et al.*, 2005), or against plant pathogenic fungi (Jin *et al.*, 2024). Biological activities usually vary depending on the molecular structure of the compound, its substitution pattern, and strains used. In this regard, benzyloxy derivatives demonstrate anti-malarial, anti-platelet, and anti-bacterial activities (Mohebi *et*

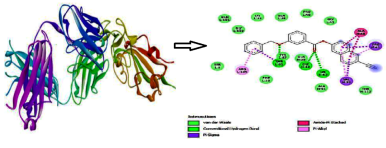

al., 2022; de Candia *et al.*, 2015; Kaushik *et al.*, 2018), while pyrimidinylphenylamine-substituted benzoyloxy derivatives are most potent in inhibiting HIV-1 (Rai *et al.*, 2023).

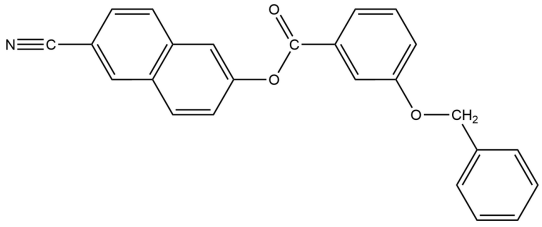

In order to explore cyanonaphthalene and (benzyloxy) benzoate groups, we have adopted these moieties for the formation of organic liquid-crystal materials (Srinivasa *et al.*, 2020). However, the toxicity of naphthalene and its potential carcinogenic properties may limit its use, and more research is needed to fully understand the mechanisms of potential action for therapeutic applications.

In the context given above, we present here the synthesis and structure elucidation of the cyanonaphthalene derivative, $C_{25}H_{17}NO_3$, (I).

2. Structural commentary

The molecular structure of (I) is shown in Fig. 1. The cyanonaphthalene moiety (C1–C10, C11≡N1) is nearly planar with an r.m.s. deviation of 0.0762 Å, with a maximum deviation of −0.138 (2) for N1. The aromatic rings of the naphthalene system are inclined towards each other with a dihedral angle of 3.82 (12)°. The torsion angles at the phenyl benzoate group (C1–O2–C12–C13) and the benzyloxy fragment (C15–O1–C19–C20) are −173.7 (2) and −174.8 (2)°, respectively, establishing an *anti*-type conformation. Otherwise, bond lengths and angles can be regarded as normal. The dihedral angle between the ten membered cyanonaphthalene ring (C1–C10) and the aromatic ring of the phenyl benzoate moiety (C13–C18) is 40.70 (10)° and between that of the benzyloxy fragments (C20–C25) is 87.51 (11)°. The dihedral angle between the phenyl rings of the phenyl benzoate and the benzyloxy systems is 72.30 (13)°.

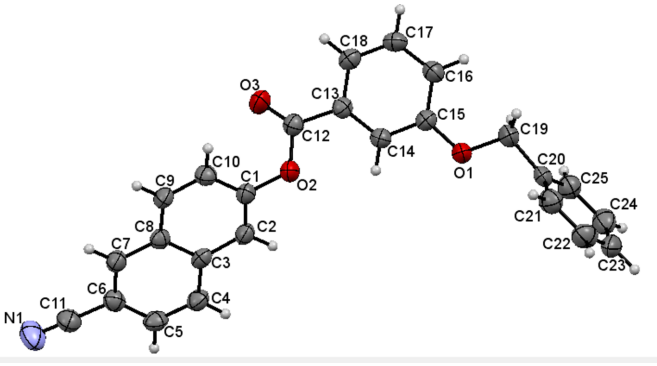

Figure 1
The molecular structure of (I) with displacement ellipsoids drawn at the 50% probability level.

Table 1
Hydrogen-bond geometry (Å, °).

*Cg*2 and *Cg*4 are the centroids of the C3–C8 and C20–C25 rings, respectively.

D—H···*A*	*D*—H	H···*A*	*D*···*A*	*D*—H···*A*
C10—H10···O2^{i}	0.93	2.68	3.579 (3)	164
C16—H16···*Cg*4^{ii}	0.93	2.97	3.711 (3)	138
C23—H23···*Cg*4^{iii}	0.93	2.76	3.611 (3)	153
C24—H24···*Cg*2^{iv}	0.93	2.98	3.858 (3)	159

Symmetry codes: (i) $-x+2, y-\frac{1}{2}, -z+1$; (ii) $x, y-1, z$; (iii) $-x+1, y+\frac{1}{2}, -z$; (iv) $-x+1, y+\frac{1}{2}, -z+1$.

3. Supramolecular features

The crystal packing of (I) includes C—H···π interactions between aromatic H atoms and phenyl rings, as detailed for the interactions C16—H16···π, C23—H23···π and C24—H24···π in Table 1 and shown in Fig. 2. There are also slipped π–π interactions in the crystal between the two aromatic rings of the naphthalene ring system [*Cg*1 and *Cg*2 are the centroids of the C1–C3/C8–C10 and = C3–C8 rings, respectively] and phenyl benzoate ring [*Cg*3 is the centroid of the C13–C18 ring], with centroid-to-centroid distances for *Cg*1···*Cg*3 and *Cg*2···*Cg*3 of 3.9699 (15) Å (slippage 1.893 Å) and 3.8569 (10) Å (slippage 1.731 Å), respectively, as shown in Fig. 3. In addition, a weak C10—H10···O2 interaction (Table 1) forming a chain parallel to [010] with an *S*(4) motif

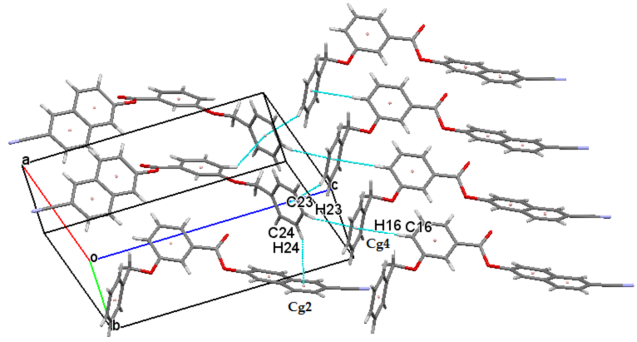

Figure 2
The molecular packing of (I) with C—H ···π interactions depicted by dashed lines.

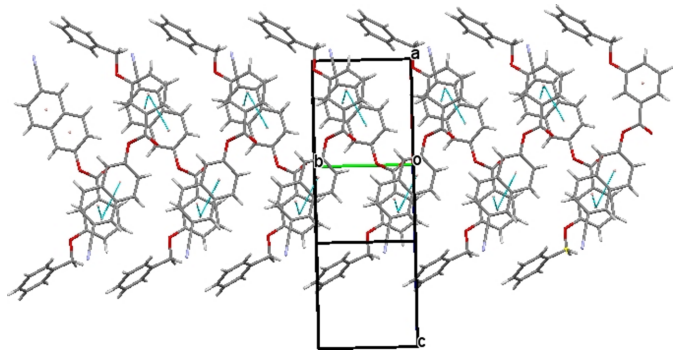

Figure 3
The molecular packing of (I) with π–π interactions depicted by pale-green dashed lines.

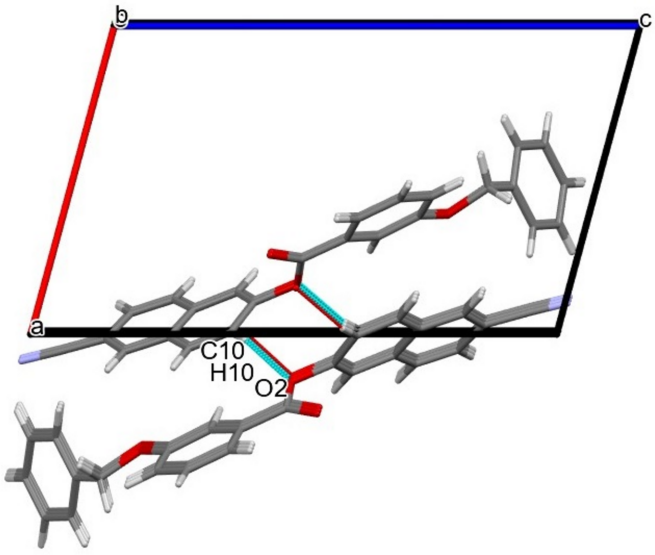

Figure 4
C—H···O interaction in (I) forming an *S*(4) chain running parallel to [010]; symmetry code as in Table 2.

(Bernstein *et al.*, 1995) is an integral part of the crystal packing (Fig. 4).

4. Hirshfeld surface analysis

Hirshfeld surface analysis (Hirshfeld, 1977; Spackman & Jayatilaka, 2009) was used to visualize and quantify intermolecular interactions using *CrystalExplorer* (Spackman *et al.*, 2021). Fig. 5 illustrates the Hirshfeld surface mapped over d_{norm}, where the colour code denotes intermolecular interactions on the Hirshfeld surface: the contacts with distances equal to the sum of the van der Waals radii are indicated in white, while those with shorter and longer distances are represented in red and blue, respectively. For (I), the C10—H10···O2 interaction is responsible for the red regions. The two-dimensional fingerprint plots indicate that the major

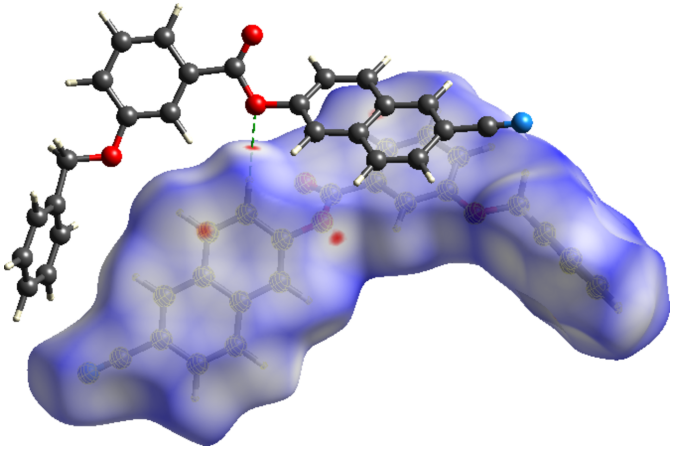

Figure 5
Hirshfeld surface of (I) plotted over d_{norm}; the dashed lines indicate the C—H···O interactions.

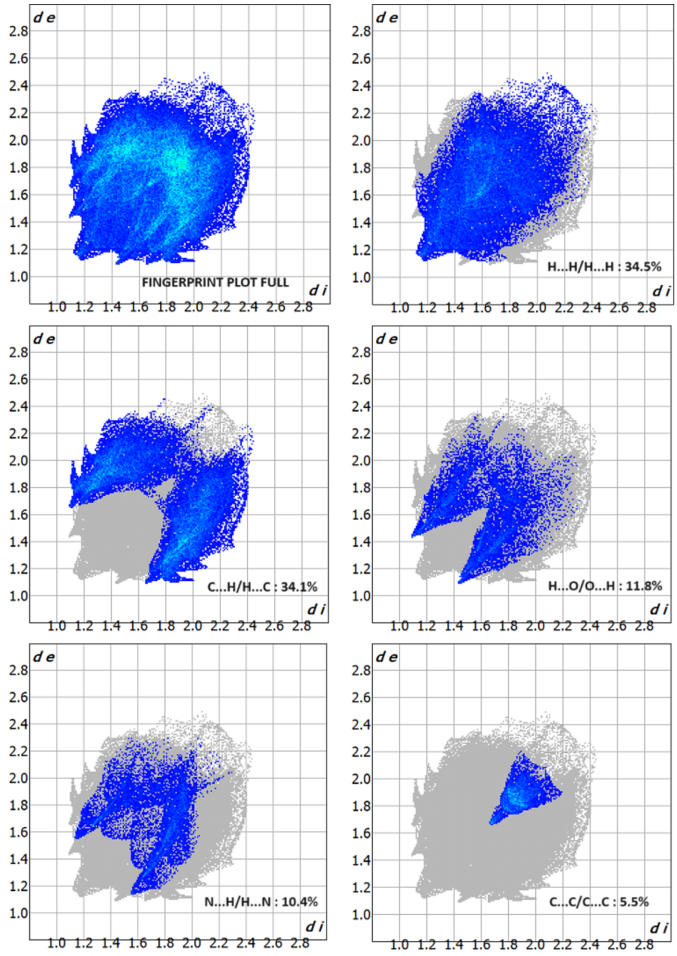

Figure 6
Two-dimensional fingerprint plots for the title compound, showing all interactions, and delineated into H···H, C···H/H···C, H···O/O···H, N···H/H···N, and C···C interactions.

contributions to the crystal packing of (I) are from H···H (34.5% contribution), C···H/H···C (34.1%), O···H/H···O (11.8%), N···H/H···N (10.4%) and C···C (5.5%) contacts, as shown in Fig. 6.

5. Density functional theory (DFT) studies

Energies were computed using the basis set B3LYP\631-G(d,p). The net interaction energies are E_{ele} = 55.2 kJ mol^{-1}, E_{pol} = 17.1 kJ mol^{-1}, E_{dis} = 218.8 kJ mol^{-1}, E_{rep} = 105.8 kJ mol^{-1} and the total interaction energy E_{tot} = 189.9 kJ mol^{-1}. The topology of energy frameworks for interaction energies are shown in Fig. 7.

The energy absorbed between bonding (HOMO) and antibonding (LUMO) orbitals determines the band gap of the material. The HOMO and LUMO were generated and their energies evaluated from the optimized structure, as shown in Fig. 8. The electron density in the HOMO of the molecule (I) mainly resides on the ester (O—C═O) group, and at the phenyl benzoate fragment to a lesser extent. In the LUMO, the electronic charge densities are delocalized to reside on the naphthalene ring and the ester group. The energies of HOMO

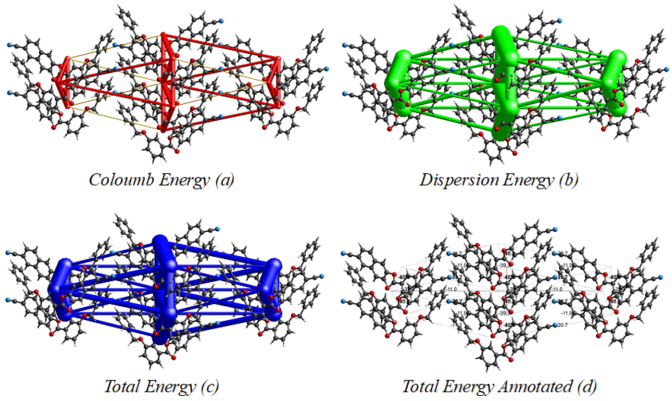

Figure 7
Energy frameworks calculated for the title compound, viewed along the *a* axis direction, showing (*a*) Coulomb potential force, (*b*) dispersion force and (*c*, *d*) total energy diagrams. The cylindrical radii are proportional to the relative strength of the corresponding energies; they were adjusted to a cutoff value of 5 kJ mol^{-1}.

and LUMO are −8.72 eV and −5.55 eV, respectively, resulting in an energy gap (E_g) of 3.17 eV. Other parameters calculated in the DFT study are compiled in Table 2.

6. Molecular Electrostatic Potential (MESP).

The molecular electrostatic potential surface (MEPS) can be used to visualize the electrostatic potential of a molecule. For (I), the MEPS is illustrated in Fig. 9, which provides possible information about the reactive sites. The electron-rich part with a partial negative charge is shown by the combination of red and pale-yellow regions on the MEPS over the nitrogen atom of the cyanonaphthalene moiety and the oxygen atom of the ester group, which is expected to undergo weak electrophilic attack. The faint blue colour spread all over the molecule implies less electron deficient parts. The absence of a bright-blue region on the MEPS reveals that there are no possible sites on the molecule for nucleophile attack (Friesner *et al.*, 2006).

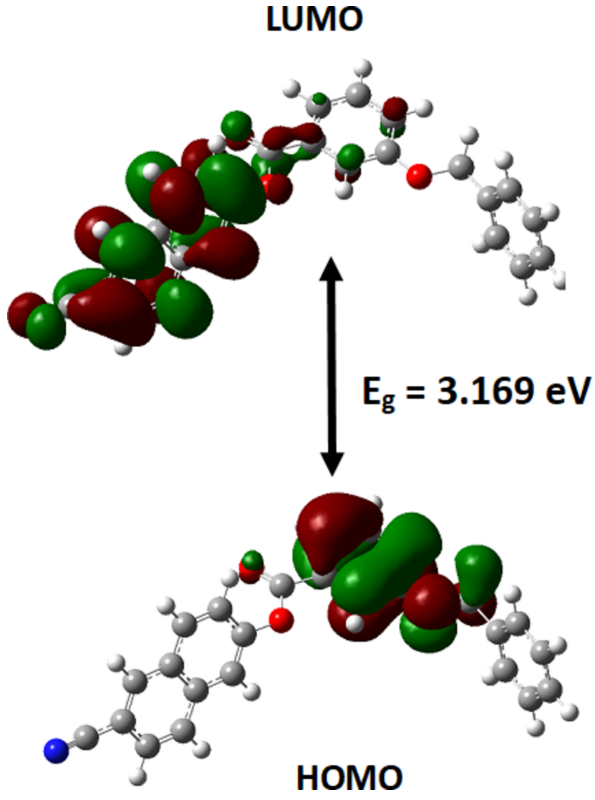

Figure 8
HOMO and LUMO of (I) with the energy band gap E_g.

Table 2
The energy values (eV) of global reactivity descriptors.

*E*_HOMO	−8.72
*E*_LUMO	−5.55
Energy gap	3.17
Ionization energy	8.72
Electron affinity	5.55
Electronegativity	7.135
Electrophilicity index	16.059
Chemical hardness	1.585
Chemical softness	0.315 eV^{-1}
Chemical potential	−7.135

7. Molecular docking studies

AutoDock Vina (Morris *et al.*, 2009) was used to carry out the docking studies. The SARS-Covid-2(PDB ID:7QF0; Planchais *et al.*, 2022) protein was selected as a receptor and the title compound as a ligand. A good binding affinity score of −9.5 kcal mol^{-1} was obtained. The interaction as generated by *Discovery Studio Visualizer* (Biovia, 2017) is shown in Fig. 10. It clearly illustrates that there are eleven hydrogen bonds and twelve van der Waals interactions between the ligand and the amino acid residues of the protein. Hence, the title molecule can be considered as a potential candidate for pharmaceutical applications.

8. Database survey

A search in the Cambridge Crystallographic Database (CSD version 2.0.4 of December 2019; Groom *et al.*. 2016) for the molecule containing a (benzyloxy)benzoate fragment resulted

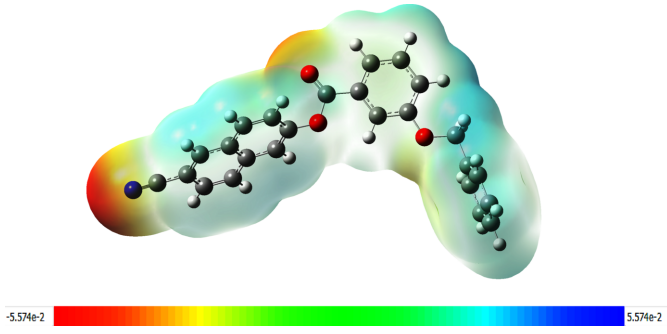

Figure 9
MEP plots of the title compound; regions of attractive potential appear in red and those of repulsive potential appear in blue.

in fourteen matches: in all these compounds, the torsion angles of the C—O—C—C unit indicate an *anti*-periplanar conformation. Among them, the compound with CCDC code VUCFEI (Harish Kumar *et al.*, 2024) is very similar to the title compound in which the cyano-biphenyl fragment is replaced by a cyano-naphthalene fragment. The search for molecules containing cyanonapthalene moieties resulted in twelve matches. In three of them, CIVZIR (Clegg *et al.*, 2008), IKUMOR (Li *et al.*, 2010) and KOPTIU (Baya *et al.*, 2015), a bulky group is attached to the cyanonaphthalene fragment, which widens the dihedral angle between the two aromatic rings of the naphthalene moiety to more than 2.57 (2)°. Otherwise the cyanonaphthalene fragment is nearly planar.

9. Synthesis and crystallization

6-Cyanonaphthalen-2-yl 4-(benzyloxy)benzoate was synthesised by the Steglich esterification reaction method between 3-benzyloxybenzoic acid and 6-hydroxy-2-naphthonitrile.

To a solution of 3-benzyloxybenzoic acid (0.228 g, 1.0 mol), 6-hydroxy-2-naphthonitrile (0.169 g, 1.0 mol) and a catalytic amount of DMAP (0.05 g) in dry dichloromethane (25 ml), DCC (0.220 g, 1. 2 mol) was added in one portion and the reaction mixture was stirred in argon medium for 12 h. The precipitate was filtered off and the filtrate was evaporated. The crude product was purified by recrystallization from chloroform, yield 65%; m.p. 396–398 K; IR: 3331, 2239, 1730, 1315, 1450, 1286, 1197, 1076, 1916, 740 cm^{-1}; ^1H NMR: 7.83 (*m*, 6H, Ar-H), 7.50 (*m*, 6H, Ar-H), 7.34 (*m*, 3H, Ar-4), 5.20 (*s*, 2H, –CH_2O) ppm; ^{13}C NMR: 169.2, 149.2, 135.7, 128.7, 123.8, 119.8, 115.6, 105.6, 71.2, 33.6, 26.124.4 ppm; elemental analysis: calculated C, 79.14; H, 4.52; N, 3.69%; found C, 79.19; H, 4.60; N, 3.75.

10. Refinement

Crystal data, data collection and structure refinement details are summarized in Table 3. H atoms were positioned geometrically (C—H = 0.93 Å) and refined as riding with $U_{iso}(H) = 1.2U_{eq}(C)$.

Table 3
Experimental details.

Crystal data	
Chemical formula	$C_{25}H_{17}NO_3$
M_r	379.39
Crystal system, space group	Monoclinic, $P2_1$
Temperature (K)	285
a, b, c (Å)	9.3141 (3), 6.7593 (2), 15.3574 (5)
β (°)	105.163 (1)
V (Å^3)	933.19 (5)
Z	2
Radiation type	Mo $K\alpha$
μ (mm^{-1})	0.09
Crystal size (mm)	0.42 × 0.31 × 0.27
Data collection	
Diffractometer	Bruker SMART APEXII CCD
Absorption correction	Multi-scan (*SADABS*; Krause *et al.*, 2015)
T_{min}, T_{max}	0.966, 0.975
No. of measured, independent and observed [$I > 2\sigma(I)$] reflections	26288, 4790, 4314
R_{int}	0.037
(sin $\theta/\lambda)_{max}$ (Å^{-1})	0.684
Refinement	
$R[F^2 > 2\sigma(F^2)]$, $wR(F^2)$, S	0.049, 0.112, 1.11
No. of reflections	4790
No. of parameters	262
No. of restraints	1
H-atom treatment	H-atom parameters constrained
$\Delta\rho_{max}$, $\Delta\rho_{min}$ (e Å^{-3})	0.18, −0.26
Absolute structure	Flack x determined using 1567 quotients $[(I^+)-(I^-)]/[(I^+)+(I^-)]$ (Parsons *et al.*, 2013)
Absolute structure parameter	0.0 (3)

Computer programs: *APEX2* and *SAINT* (Bruker, 2017), *SHELXT* (Sheldrick, 2015*a*), *SHELXL* (Sheldrick, 2015*b*), *Mercury* (Macrae *et al.*, 2020) and *publCIF* (Westrip, 2010).

Acknowledgements

The authors acknowledge the SSCU, Indian Institute Science, Bangalore, for constant support in extending the SC-XRD facility. The authors are thankful to BSPMs lab for use of their

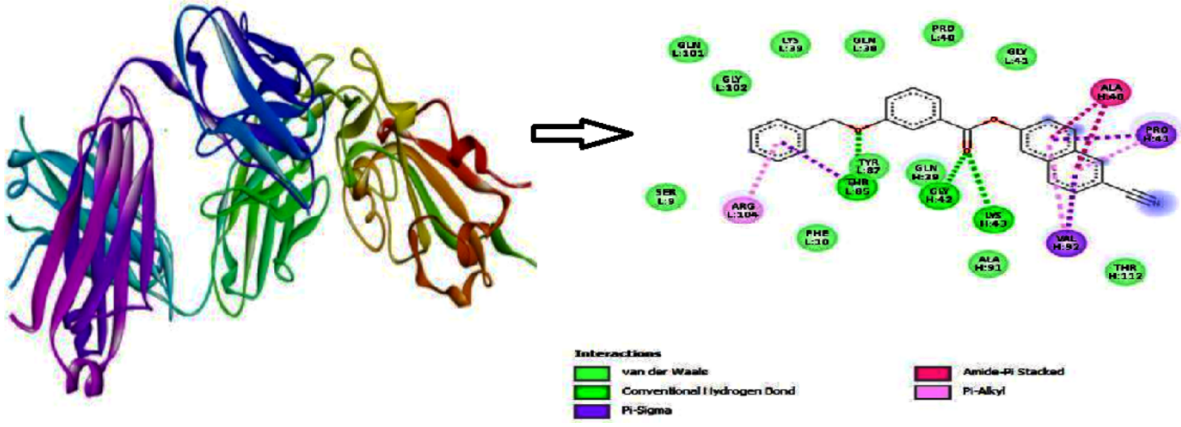

Figure 10
A three-dimensional view of the SARS-Covid-2(PDB ID:7QF0) protein and two-dimensional view of the molecular interaction between the ligand and amino acid residues.

computing facilities. MH is grateful to the Department of PG Studies and Research in Physics, Albert Einstein Block, UCS, Tumkur University, Tumkur.

Funding information

Funding for this research was provided by: Vission Group of Science and Technology (award No. GRD319 to Palakshamurthy BS).

References

Ashraf, K., Yasrebi, K., Adeniyi, E. T., Hertlein, T., Ohlsen, K., Lalk, M., Erdmann, F. & Hilgeroth, A. (2019). *Drug. Des. Dev. Ther.* **13**, 275–283.

Baya, M., Belío, Ú., Forniés, J., Martín, A., Perálvarez, M. & Sicilia, V. (2015). *Inorg. Chim. Acta*, **424**, 136–149.

Bernstein, J., Davis, R. E., Shimoni, L. & Chang, N.-L. (1995). *Angew. Chem. Int. Ed. Engl.* **34**, 1555–1573.

Biovia (2017). *Discovery Studio Visualizer*. Biovia, San Diego, CA, USA.

Boyle, E. A., Freemanm, P. C., Mangan, F. R. & Thomson, M. J. (1982). *J. Pharm. Pharmacol.* **34**, 562–569.

Bruker (2017). *APEX2* and *SAINT*. Bruker AXS Inc., Madison, Wisconsin, USA.

Candia, M. de, Marini, E., Zaetta, G., Cellamare, S., Di Stilo, A. & Altomare, C. D. (2015). *Eur. J. Pharm. Sci.* **72**, 69–80.

Clegg, W., Dale, S., Hevia, E., Hogg, L., Honeyman, G., Mulvey, R., O'Hara, C. & Russo, L. (2008). *Angew. Chem. Int. Ed.* **47**, 731–734.

Das, S. K., Panda, G., Chaturvedi, V., Manju, Y. S., Gaikwad, A. K. & Sinha, S. (2007). *Bioorg. Med. Chem. Lett.* **17**, 5586–5589.

El-Desoky, E.-S. I., Keshk, E. M., El-Sawi, A. A., Abozeid, M. A., Abouzeid, L. A. & Abdel-Rahman, A.-R. H. (2018). *Saudi Pharm. J.* **26**, 852–859.

Friesner, R. A., Murphy, R. B., Repasky, M. P., Frye, L. L., Greenwood, J. R., Halgren, T. A., Sanschagrin, P. C. & Mainz, D. T. (2006). *J. Med. Chem.* **49**, 6177–6196.

Groom, C. R., Bruno, I. J., Lightfoot, M. P. & Ward, S. C. (2016). *Acta Cryst.* B**72**, 171–179.

Harish Kumar, M., Vinduvahini, M., Devarajegowda, H. C., Srinivasa, H. T. & Palakshamurthy, B. S. (2024). *Acta Cryst.* E**80**, 1010–1013.

Hekal, M., Abdalha, A. A., Farag, H. & Ali, A. T. (2024). *Chem. Biodivers.* pp. e202401023.

Hirshfeld, H. L. (1977). *Theor. Chim. Acta*, **44**, 129–138.

Jin, F., Peng, F., Li, W. R., Chai, J. Q., Chen, M., Lu, A. M. & Zhou, M. G. (2024). *J. Saudi Chem. Soc.* **28**, 101928.

Kaushik, C. P., Pahwa, A., Kumar, D., Kumar, A., Singh, D., Kumar, K. & Luxmi, R. (2018). *J. Heterocycl. Chem.* **55**, 1720–1728.

Krause, L., Herbst-Irmer, R., Sheldrick, G. M. & Stalke, D. (2015). *J. Appl. Cryst.* **48**, 3–10.

Li, T., García, J. J., Brennessel, W. W. & Jones, W. D. (2010). *Organometallics*, **29**, 2430–2445.

Macrae, C. F., Sovago, I., Cottrell, S. J., Galek, P. T. A., McCabe, P., Pidcock, E., Platings, M., Shields, G. P., Stevens, J. S., Towler, M. & Wood, P. A. (2020). *J. Appl. Cryst.* **53**, 226–235.

Mohebi, M., Fayazi, N., Esmaeili, S., Rostami, M., Bagheri, F., Aliabadi, A., Asadi, P. & Saghaie, L. (2022). *Res. Pharma Sci.* **17**, 252–264.

Morris, G. M., Huey, R., Lindstrom, W., Sanner, M. F., Belew, R. K., Goodsell, D. S. & Olson, A. J. (2009). *J. Comput. Chem.* **30**, 27852791.

Özdemir, Z., Sari, S., Karakurt, A. & Dalkara, S. (2019). *Drug Dev. Res.* **80**, 269–280.

Parsons, S., Flack, H. D. & Wagner, T. (2013). *Acta Cryst.* B**69**, 249–259.

Perrone, R., Doria, F., Butovskaya, E., Frasson, I., Botti, S., Scalabrin, M., Lago, S., Grande, V., Nadai, M., Freccero, M. & Richter, S. N. (2015). *J. Med. Chem.* **58**, 9639–9652.

Planchais, C., Fernández, I., Bruel, T., de Melo, G. D., Prot, M., Beretta, M., Guardado-Calvo, P., Dufloo, J., Molinos-Albert, L. M., Backovic, M., Chiaravalli, J., Giraud, E., Vesin, B., Conquet, L., Grzelak, L., Planas, D., Staropoli, I., Guivel-Benhassine, F., Hieu, T., Boullé, M., Cervantes-Gonzalez, M., Ungeheuer, M., Charneau, P., van der Werf, S., Agou, F., Bartoli, M., Diallo, A., Le Mestre, S., Paul, C., Petrov-Sanchez, V., Yazdanpanah, Y., Ficko, C., Chirouze, C., Andrejak, C., Malvy, D., Goehringer, F., Rossignol, P., Gigante, T., Gilg, M., Rossignol, B., Etienne, M., Beluze, M., Bachelet, D., Bhavsar, K., Bouadma, L., Cervantes-Gonzalez, M., Chair, A., Charpentier, C., Chenard, L., Couffignal, C., Debray, M., Descamps, D., Duval, X., Eloy, P., Esposito-Farese, M., Florence, A., Ghosn, J., Hoffmann, I., Kafif, O., Khalil, A., Lafhej, N., Laouénan, C., Laribi, S., Le, M., Le Hingrat, Q., Letrou, S., Mentré, F., Peytavin, G., Piquard, V., Roy, C., Schneider, M., Su, R., Tardivon, C., Timsit, J., Tubiana, S., Visseaux, B., Deplanque, D., Hulot, J., Diehl, J., Picone, O., Angoulvant, F., Abrous, A., Couffin-Cadiergues, S., Da Silva, F. D., Esperou, H., Houas, I., Jaafoura, S., Papadopoulos, A., Gaymard, A., Lina, B., Rosa-Calatrava, M., Dorival, C., Guedj, J., Lingas, G., Neant, N., Abel, L., Manda, V., Behillil, S., Enouf, V., Levy, Y., Wiedemann, A., Arowas, L., Perlaza, B. L., Perrin de Facci, L., Chaouche, S., Sangari, L., Renaudat, C., Fernandes Pellerin, S., van Platen, C., Jolly, N., Kuhmel, L., Garaud, V., Rafanoson, H., Gardais, S., de Parseval, N., Dugast, C., Jannet, C., Ropars, S., Momboisse, F., Porteret, I., Cailleau, I., Hoen, B., Tondeur, L., Besombes, C., Fontanet, A., Dimitrov, J. D., Simon-Lorière, E., Bourhy, H., Montagutelli, X., Rey, F. A., Schwartz, O. & Mouquet, H. (2022). *J. Exp. Med.* **219**, e20220638.

Prakash, N., Elamaran, M. & Ingarsal, N. (2015). *Chem. Sci. Trans.* **4**, 947–954.

Rai, D., Chen, W., Tian, Y., Chen, X., Zhan, P., De Clercq, E., Pannecouque, C., Balzarini, J. & Liu, X. (2023). *Bioorg. Med. Chem.* **21**, 7398–7405.

Sheldrick, G. M. (2015*a*). *Acta Cryst.* A**71**, 3–8.

Sheldrick, G. M. (2015*b*). *Acta Cryst.* C**71**, 3–8.

Spackman, M. A. & Jayatilaka, D. (2009). *CrystEngComm*, **11**, 19–32.

Spackman, P. R., Turner, M. J., McKinnon, J. J., Wolff, S. K., Grimwood, D. J., Jayatilaka, D. & Spackman, M. A. (2021). *J. Appl. Cryst.* **54**, 1006–1011.

Srinivasa, H. T., Prutha, N. & Pratibha, R. (2020). *J. Mol. Struct.* **1199**, 126971.

Valente, S., Trisciuoglio, D., De Luca, T., Nebbioso, A., Labella, D., Lenoci, A., Bigogno, C., Dondio, G., Miceli, M., Brosch, G., Del Bufalo, D., Altucci, L. & Mai, A. (2014). *J. Med. Chem.* **57**, 6259–6265.

Voets, M., Antes, I., Scherer, C., Müller-Vieira, U., Biemel, K., Barassin, C., Marchais-Oberwinkler, S. & Hartmann, R. W. (2005). *J. Med. Chem.* **48**, 6632–6642.

Westrip, S. P. (2010). *J. Appl. Cryst.* **43**, 920–925.

supporting information

Acta Cryst. (2024). E**80**, 1180-1185 [https://doi.org/10.1107/S2056989024009964]

Crystal structure, Hirshfeld surface analysis, and DFT and molecular docking studies of 6-cyanonaphthalen-2-yl 4-(benzyloxy)benzoate

Mahadevaiah Harish Kumar, Shivakumar Santhosh Kumar, Hirehalli Chikkegowda Devarajegowda, Hosapalya Thimmaiah Srinivasa and Bandrehalli Siddagangaiah Palakshamurthy

Computing details

6-Cyanonaphthalen-2-yl 4-(benzyloxy)benzoate

Crystal data

$C_{25}H_{17}NO_3$
M_r = 379.39
Monoclinic, $P2_1$
Hall symbol: P 2yb
a = 9.3141 (3) Å
b = 6.7593 (2) Å
c = 15.3574 (5) Å
β = 105.163 (1)°
V = 933.19 (5) Å^3
Z = 2
$F(000)$ = 396
D_x = 1.350 Mg m^{-3}
Melting point: 386 K
Mo $K\alpha$ radiation, λ = 0.71073 Å
Cell parameters from 2709 reflections
θ = 2.9–29.0°
μ = 0.09 mm^{-1}
T = 285 K
Prism, colourless
0.42 × 0.31 × 0.27 mm

Data collection

Bruker SMART APEXII CCD diffractometer
Radiation source: fine-focus sealed tube
Graphite monochromator
Detector resolution: 0.012 pixels mm^{-1}
φ and Ω scans
Absorption correction: multi-scan (*SADABS*; Krause *et al.*, 2015)
T_{min} = 0.966, T_{max} = 0.975
26288 measured reflections
4790 independent reflections
4314 reflections with $I > 2\sigma(I)$
R_{int} = 0.037
θ_{max} = 29.1°, θ_{min} = 2.9°
h = −12→12
k = −8→9
l = −20→21

Refinement

Refinement on F^2
Least-squares matrix: full
$R[F^2 > 2\sigma(F^2)]$ = 0.049
$wR(F^2)$ = 0.112
S = 1.11
4790 reflections
262 parameters
1 restraint
0.012 constraints
Primary atom site location: structure-invariant direct methods
Secondary atom site location: difference Fourier map
Hydrogen site location: inferred from neighbouring sites
H-atom parameters constrained
$w = 1/[\sigma^2(F_o^2) + (0.0503P)^2 + 0.1406P]$ where $P = (F_o^2 + 2F_c^2)/3$
$(\Delta/\sigma)_{max} < 0.001$
$\Delta\rho_{max}$ = 0.18 e Å^{-3}
$\Delta\rho_{min}$ = −0.26 e Å^{-3}

Absolute structure: Flack *x* determined using 1567 quotients $[(I^+)-(I^-)]/[(I^+)+(I^-)]$ (Parsons *et al.*, 2013)
Absolute structure parameter: 0.0 (3)

Special details

Geometry. All esds (except the esd in the dihedral angle between two l.s. planes) are estimated using the full covariance matrix. The cell esds are taken into account individually in the estimation of esds in distances, angles and torsion angles; correlations between esds in cell parameters are only used when they are defined by crystal symmetry. An approximate (isotropic) treatment of cell esds is used for estimating esds involving l.s. planes.

Fractional atomic coordinates and isotropic or equivalent isotropic displacement parameters (Å²)

	x	*y*	*z*	U_{iso}*/U_{eq}
O1	0.6200 (2)	0.4858 (3)	0.73167 (12)	0.0472 (5)
O2	0.8441 (2)	0.3738 (3)	0.48087 (11)	0.0429 (4)
O3	0.7449 (2)	0.0904 (3)	0.41447 (13)	0.0562 (5)
N1	1.0966 (4)	0.8151 (5)	−0.00409 (19)	0.0720 (8)
C20	0.5314 (3)	0.6692 (4)	0.84087 (16)	0.0404 (5)
C25	0.4012 (3)	0.7744 (5)	0.82984 (18)	0.0484 (6)
H25	0.314701	0.729814	0.789327	0.058*
C24	0.3981 (3)	0.9466 (5)	0.8788 (2)	0.0545 (7)
H24	0.309367	1.015313	0.871917	0.065*
C23	0.5259 (4)	1.0150 (5)	0.93713 (17)	0.0519 (7)
H23	0.524380	1.130395	0.969887	0.062*
C22	0.6562 (3)	0.9121 (5)	0.94689 (19)	0.0559 (7)
H22	0.743250	0.959386	0.985945	0.067*
C21	0.6599 (3)	0.7402 (5)	0.8998 (2)	0.0510 (7)
H21	0.748828	0.671363	0.907589	0.061*
C19	0.5315 (3)	0.4734 (4)	0.7946 (2)	0.0522 (7)
H19A	0.571340	0.372032	0.839136	0.063*
H19B	0.430467	0.436973	0.763393	0.063*
C15	0.6204 (3)	0.3220 (4)	0.67884 (16)	0.0369 (5)
C14	0.6894 (3)	0.3444 (4)	0.60972 (16)	0.0362 (5)
H14	0.733653	0.464269	0.602097	0.043*
C13	0.6925 (2)	0.1874 (4)	0.55184 (15)	0.0348 (5)
C18	0.6267 (3)	0.0076 (4)	0.56294 (16)	0.0413 (5)
H18	0.627027	−0.096681	0.523488	0.050*
C17	0.5613 (3)	−0.0141 (4)	0.63296 (18)	0.0473 (6)
H17	0.519366	−0.135115	0.641378	0.057*
C16	0.5568 (3)	0.1408 (4)	0.69109 (18)	0.0441 (6)
H16	0.511664	0.124155	0.737942	0.053*
C12	0.7611 (3)	0.2051 (4)	0.47543 (16)	0.0387 (5)
C1	0.9033 (3)	0.4198 (4)	0.40816 (15)	0.0369 (5)
C10	0.9968 (3)	0.2840 (4)	0.37968 (16)	0.0400 (5)
H10	1.020892	0.163273	0.408940	0.048*
C9	1.0511 (3)	0.3335 (4)	0.30832 (16)	0.0377 (5)
H9	1.112080	0.244941	0.288451	0.045*
C8	1.0162 (2)	0.5176 (4)	0.26402 (14)	0.0338 (5)

C3	0.9284 (2)	0.6563 (3)	0.29738 (15)	0.0342 (5)
C2	0.8722 (3)	0.6006 (4)	0.37101 (16)	0.0386 (5)
H2	0.814018	0.688432	0.393638	0.046*
C7	1.0641 (3)	0.5664 (4)	0.18674 (16)	0.0391 (5)
H7	1.121836	0.477536	0.164345	0.047*
C4	0.8978 (3)	0.8423 (4)	0.25446 (17)	0.0419 (5)
H4	0.845363	0.936274	0.277969	0.050*
C5	0.9433 (3)	0.8867 (4)	0.17954 (17)	0.0435 (6)
H5	0.920636	1.008990	0.151554	0.052*
C6	1.0253 (3)	0.7458 (4)	0.14457 (16)	0.0403 (5)
C11	1.0668 (3)	0.7861 (4)	0.06199 (19)	0.0496 (6)

Atomic displacement parameters (Å²)

	U^{11}	U^{22}	U^{33}	U^{12}	U^{13}	U^{23}
O1	0.0643 (11)	0.0366 (10)	0.0515 (10)	−0.0114 (8)	0.0341 (9)	−0.0087 (8)
O2	0.0574 (10)	0.0396 (10)	0.0374 (9)	−0.0067 (8)	0.0224 (8)	−0.0056 (7)
O3	0.0713 (13)	0.0535 (12)	0.0519 (11)	−0.0164 (10)	0.0305 (10)	−0.0191 (10)
N1	0.097 (2)	0.070 (2)	0.0591 (15)	0.0155 (17)	0.0381 (15)	0.0228 (14)
C20	0.0513 (14)	0.0390 (13)	0.0384 (12)	−0.0067 (11)	0.0251 (10)	−0.0015 (10)
C25	0.0464 (14)	0.0527 (17)	0.0452 (14)	−0.0026 (12)	0.0104 (11)	−0.0016 (12)
C24	0.0602 (17)	0.0483 (17)	0.0603 (17)	0.0132 (13)	0.0250 (14)	0.0054 (13)
C23	0.082 (2)	0.0397 (14)	0.0416 (13)	−0.0051 (14)	0.0290 (13)	−0.0055 (11)
C22	0.0584 (17)	0.0583 (18)	0.0483 (15)	−0.0152 (15)	0.0093 (13)	−0.0055 (13)
C21	0.0429 (13)	0.0525 (17)	0.0608 (16)	−0.0015 (12)	0.0193 (12)	−0.0012 (13)
C19	0.0694 (18)	0.0414 (16)	0.0587 (16)	−0.0104 (13)	0.0396 (14)	−0.0078 (12)
C15	0.0416 (12)	0.0332 (12)	0.0376 (11)	−0.0022 (9)	0.0135 (10)	−0.0029 (9)
C14	0.0411 (12)	0.0320 (12)	0.0370 (11)	−0.0026 (9)	0.0130 (9)	0.0010 (9)
C13	0.0360 (11)	0.0375 (13)	0.0310 (10)	0.0004 (9)	0.0086 (8)	0.0000 (9)
C18	0.0466 (13)	0.0359 (13)	0.0413 (12)	−0.0042 (11)	0.0113 (10)	−0.0070 (10)
C17	0.0545 (14)	0.0364 (14)	0.0532 (14)	−0.0126 (12)	0.0181 (12)	−0.0017 (11)
C16	0.0517 (14)	0.0433 (15)	0.0422 (13)	−0.0091 (11)	0.0210 (11)	−0.0009 (10)
C12	0.0416 (12)	0.0394 (13)	0.0355 (11)	−0.0010 (10)	0.0110 (9)	−0.0025 (10)
C1	0.0422 (12)	0.0380 (13)	0.0329 (11)	−0.0050 (10)	0.0138 (9)	−0.0054 (9)
C10	0.0470 (13)	0.0340 (12)	0.0395 (12)	0.0020 (10)	0.0123 (10)	0.0035 (10)
C9	0.0425 (12)	0.0342 (12)	0.0386 (11)	0.0037 (10)	0.0145 (10)	−0.0037 (9)
C8	0.0338 (10)	0.0347 (12)	0.0322 (10)	−0.0009 (9)	0.0076 (8)	−0.0033 (9)
C3	0.0372 (11)	0.0304 (11)	0.0339 (11)	0.0000 (9)	0.0072 (9)	−0.0063 (9)
C2	0.0436 (13)	0.0362 (13)	0.0379 (11)	0.0007 (10)	0.0140 (10)	−0.0079 (10)
C7	0.0423 (12)	0.0385 (13)	0.0382 (11)	0.0017 (10)	0.0132 (10)	−0.0032 (10)
C4	0.0504 (13)	0.0319 (13)	0.0446 (13)	0.0043 (10)	0.0143 (11)	−0.0043 (10)
C5	0.0542 (14)	0.0316 (13)	0.0423 (12)	0.0022 (11)	0.0082 (11)	0.0040 (10)
C6	0.0450 (13)	0.0411 (14)	0.0344 (11)	−0.0049 (11)	0.0096 (10)	0.0012 (10)
C11	0.0583 (16)	0.0443 (15)	0.0469 (14)	0.0027 (12)	0.0149 (12)	0.0083 (12)

Geometric parameters (Å, º)

O1—C15	1.373 (3)	C13—C12	1.481 (3)
O1—C19	1.427 (3)	C18—C17	1.375 (3)
O2—C12	1.368 (3)	C18—H18	0.9300
O2—C1	1.404 (3)	C17—C16	1.384 (4)
O3—C12	1.194 (3)	C17—H17	0.9300
N1—C11	1.137 (4)	C16—H16	0.9300
C20—C25	1.378 (4)	C1—C2	1.348 (4)
C20—C21	1.384 (4)	C1—C10	1.412 (3)
C20—C19	1.502 (4)	C10—C9	1.363 (3)
C25—C24	1.390 (4)	C10—H10	0.9300
C25—H25	0.9300	C9—C8	1.415 (3)
C24—C23	1.369 (4)	C9—H9	0.9300
C24—H24	0.9300	C8—C7	1.412 (3)
C23—C22	1.373 (4)	C8—C3	1.424 (3)
C23—H23	0.9300	C3—C4	1.413 (3)
C22—C21	1.374 (4)	C3—C2	1.416 (3)
C22—H22	0.9300	C2—H2	0.9300
C21—H21	0.9300	C7—C6	1.378 (4)
C19—H19A	0.9700	C7—H7	0.9300
C19—H19B	0.9700	C4—C5	1.360 (4)
C15—C14	1.386 (3)	C4—H4	0.9300
C15—C16	1.395 (4)	C5—C6	1.412 (4)
C14—C13	1.389 (3)	C5—H5	0.9300
C14—H14	0.9300	C6—C11	1.445 (4)
C13—C18	1.391 (4)		

C15—O1—C19	116.41 (19)	C17—C16—C15	119.4 (2)
C12—O2—C1	118.01 (18)	C17—C16—H16	120.3
C25—C20—C21	119.0 (3)	C15—C16—H16	120.3
C25—C20—C19	120.4 (3)	O3—C12—O2	122.9 (2)
C21—C20—C19	120.5 (3)	O3—C12—O2	122.9 (2)
C20—C25—C24	120.5 (3)	O3—C12—C13	125.2 (2)
C20—C25—H25	119.7	O2—C12—C13	111.91 (19)
C24—C25—H25	119.7	O2—C12—C13	111.91 (19)
C23—C24—C25	120.0 (3)	C2—C1—O2	116.9 (2)
C23—C24—H24	120.0	C2—C1—O2	116.9 (2)
C25—C24—H24	120.0	C2—C1—C10	122.7 (2)
C24—C23—C22	119.5 (3)	O2—C1—C10	120.3 (2)
C24—C23—H23	120.3	O2—C1—C10	120.3 (2)
C22—C23—H23	120.3	C9—C10—C1	118.5 (2)
C23—C22—C21	121.0 (3)	C9—C10—H10	120.7
C23—C22—H22	119.5	C1—C10—H10	120.7
C21—C22—H22	119.5	C10—C9—C8	121.1 (2)
C22—C21—C20	120.1 (3)	C10—C9—H9	119.5
C22—C21—H21	120.0	C8—C9—H9	119.5
C20—C21—H21	120.0	C7—C8—C9	121.7 (2)

O1—C19—C20	109.9 (2)	C7—C8—C3	119.1 (2)
O1—C19—H19A	109.7	C9—C8—C3	119.2 (2)
C20—C19—H19A	109.7	C4—C3—C2	122.5 (2)
O1—C19—H19B	109.7	C4—C3—C8	118.8 (2)
C20—C19—H19B	109.7	C2—C3—C8	118.6 (2)
H19A—C19—H19B	108.2	C1—C2—C3	119.7 (2)
O1—C15—C14	116.0 (2)	C1—C2—H2	120.1
O1—C15—C16	124.1 (2)	C3—C2—H2	120.1
C14—C15—C16	119.9 (2)	C6—C7—C8	119.9 (2)
C15—C14—C13	119.9 (2)	C6—C7—H7	120.0
C15—C14—H14	120.1	C8—C7—H7	120.0
C13—C14—H14	120.1	C5—C4—C3	121.4 (2)
C14—C13—C18	120.4 (2)	C5—C4—H4	119.3
C14—C13—C12	122.0 (2)	C3—C4—H4	119.3
C18—C13—C12	117.6 (2)	C4—C5—C6	119.5 (2)
C17—C18—C13	119.2 (2)	C4—C5—H5	120.3
C17—C18—H18	120.4	C6—C5—H5	120.3
C13—C18—H18	120.4	C7—C6—C5	121.1 (2)
C18—C17—C16	121.2 (2)	C7—C6—C11	118.8 (2)
C18—C17—H17	119.4	C5—C6—C11	120.1 (2)
C16—C17—H17	119.4	N1—C11—C6	178.3 (3)

C21—C20—C25—C24	−1.5 (4)	C14—C13—C12—O2	12.4 (3)
C19—C20—C25—C24	174.2 (2)	C18—C13—C12—O2	−169.2 (2)
C20—C25—C24—C23	1.3 (4)	O2—O2—C1—C2	0.0 (4)
C25—C24—C23—C22	−0.2 (4)	C12—O2—C1—C2	125.9 (2)
C24—C23—C22—C21	−0.8 (4)	C12—O2—C1—O2	0 (100)
C23—C22—C21—C20	0.6 (4)	O2—O2—C1—C10	0.0 (4)
C25—C20—C21—C22	0.5 (4)	C12—O2—C1—C10	−57.1 (3)
C19—C20—C21—C22	−175.1 (2)	C2—C1—C10—C9	−3.8 (4)
C15—O1—C19—C20	−174.8 (2)	O2—C1—C10—C9	179.5 (2)
C25—C20—C19—O1	116.3 (3)	O2—C1—C10—C9	179.5 (2)
C21—C20—C19—O1	−68.1 (3)	C1—C10—C9—C8	0.6 (4)
C19—O1—C15—C14	171.5 (2)	C10—C9—C8—C7	−176.2 (2)
C19—O1—C15—C16	−8.5 (4)	C10—C9—C8—C3	2.9 (3)
O1—C15—C14—C13	−178.7 (2)	C7—C8—C3—C4	−2.8 (3)
C16—C15—C14—C13	1.2 (3)	C9—C8—C3—C4	178.1 (2)
C15—C14—C13—C18	−0.1 (3)	C7—C8—C3—C2	175.6 (2)
C15—C14—C13—C12	178.3 (2)	C9—C8—C3—C2	−3.4 (3)
C14—C13—C18—C17	−1.3 (4)	O2—C1—C2—C3	−179.9 (2)
C12—C13—C18—C17	−179.7 (2)	O2—C1—C2—C3	−179.9 (2)
C13—C18—C17—C16	1.5 (4)	C10—C1—C2—C3	3.2 (4)
C18—C17—C16—C15	−0.4 (4)	C4—C3—C2—C1	178.9 (2)
O1—C15—C16—C17	178.9 (2)	C8—C3—C2—C1	0.5 (3)
C14—C15—C16—C17	−1.0 (4)	C9—C8—C7—C6	178.8 (2)
O2—O2—C12—O3	0.00 (4)	C3—C8—C7—C6	−0.3 (3)
C1—O2—C12—O3	4.7 (4)	C2—C3—C4—C5	−174.8 (2)
C1—O2—C12—O2	0 (100)	C8—C3—C4—C5	3.6 (3)

O2—O2—C12—C13	0.00 (7)	C3—C4—C5—C6	−1.2 (4)
C1—O2—C12—C13	−173.7 (2)	C8—C7—C6—C5	2.8 (4)
C14—C13—C12—O3	−166.0 (3)	C8—C7—C6—C11	−175.6 (2)
C18—C13—C12—O3	12.5 (4)	C4—C5—C6—C7	−2.1 (4)
C14—C13—C12—O2	12.4 (3)	C4—C5—C6—C11	176.3 (2)
C18—C13—C12—O2	−169.2 (2)		

Hydrogen-bond geometry (Å, º)

*Cg*2 and *Cg*4 are the centroids of the C3–C8 and C20–C25 rings, respectively.

D—H···*A*	*D*—H	H···*A*	*D*···*A*	*D*—H···*A*
C10—H10···O2^{i}	0.93	2.68	3.579 (3)	164
C16—H16···*Cg*4^{ii}	0.93	2.97	3.711 (3)	138
C23—H23···*Cg*4^{iii}	0.93	2.76	3.611 (3)	153
C24—H24···*Cg*2^{iv}	0.93	2.98	3.858 (3)	159

Symmetry codes: (i) −*x*+2, *y*−1/2, −*z*+1; (ii) *x*, *y*−1, *z*; (iii) −*x*+1, *y*+1/2, −*z*; (iv) −*x*+1, *y*+1/2, −*z*+1.